Solution Properties of Cellulose Tris(phenyl carbamate). 1. Characterization of the Conformation and Intermolecular Interaction

Fumio Kasabo, Takayuki Kanematsu, Tomo Nakagawa, and Takahiro Sato*,†

Department of Macromolecular Science, Osaka University, 1-1 Machikaneyama-cho, Toyonaka, Osaka 560-0043, Japan

Akio Teramoto

Research Organization of Science and Engineering, Ritsumeikan University, and CREST of Japan Science and Technology, Nojihigashi 1-1-1, Kusatsu, Siga 525-8577, Japan

Received August 24, 1999; Revised Manuscript Received February 1, 2000

ABSTRACT: The radius of gyration $\langle S^2\rangle^{1/2}$, hydrodynamic radius R_H, intrinsic viscosity $[\eta]$, and second virial coefficient A_2 for cellulose tris(phenyl carbamate) (CTC) in tetrahydrofuran (THF) at 25 °C were determined in a wide range of molecular weights, 1.91×10^4 to 392×10^4, by static and dynamic light scattering and viscometry. Furthermore, the osmotic compressibility $\partial c/\partial\Pi$ for isotropic THF solutions of CTC samples was measured at 25 °C by static light scattering over wide ranges of the polymer concentration. Data of $\langle S^2\rangle^{1/2}$, R_H, and $[\eta]$ were analyzed by the established quasi-two parameter theory for the wormlike chain model to determine the molar mass M_L per unit contour length and the persistence length q. On the other hand, results of A_2 and $\partial c/\partial\Pi$ were analyzed on the basis of the scaled particle theory for wormlike spherocylinders combined with the quasi-two parameter theory for A_2 to estimate the hard-core diameter d_0 and strength δ of the soft dispersion force of the CTC chain in THF. The value of M_L [=1040 (±70) nm^{-1}] estimated is consistent with the $^3/_2$ helical conformation of CTC in the crystal of the CTC-methyl ethyl ketone complex, while the hard-core diameter d_0 [=1.4 (±0.1) nm] is slightly smaller than the interchain spacing (=1.66 nm) of CTC in the same crystal. The value of q [=10.5 (±1) nm] for CTC is comparable to literature values of q for some other cellulose derivatives reported so far.

1. Introduction

Solution properties of stiff or semiflexible polymers are distinct from those of flexible polymers. When the molecular weight of a stiff polymer is not too high, the radius of gyration, intrinsic viscosity, diffusion coefficient, and sedimentation coefficient are free from the intramolecular excluded-volume effect even in a good solvent,[1] and the second virial coefficient is essentially independent of the molecular weight, which demonstrates that effects of multiple contacts between two polymer chains are not appreciable.[2] With respect to concentrated solution properties, stiff polymers possess abilities of lyotropic liquid-crystal formation and strong viscosity enhancement,[3] in contrast with flexible polymers.

Cellulose derivatives are intermediate between flexible polymers and typical stiff polymers. They possess lyotropic liquid crystallinity,[4] but their conformation can be appreciably perturbed by the intramolecular excluded-volume effect.[5] In fact, there were historical disputes as to whether their extended chain conformation comes from the excluded volume effect or the chain stiffness effect.[6,7]

Owing to their intermediate chain stiffness, cellulose derivatives are suitable to study the crossover behavior of solution properties between flexible and stiff polymers. The main purpose of our present investigation on cellulose derivatives is to elucidate this crossover behavior. We have chosen cellulose tris(phenyl carbamate) (or cellulose tricarbanilate, CTC) as the test sample to study its dilute through concentrated solution properties. CTC is one of the most extensively studied cellulose derivatives, and it is suitable to make quantitative arguments on its solution properties, because CTC is readily prepared and fractionated to obtain test samples with perfect substitution and narrow molecular weight distribution and also has a good solubility to common organic solvents.

The present paper (part 1 of this series of papers) is concerned with the characterization of the chain conformation and intermolecular interaction of CTC in tetrahydrofuran (THF) at 25 °C. The conformation is characterized by the analyses of data of the radius of gyration, hydrodynamic radius (calculated from the diffusion coefficient), and intrinsic viscosity on the basis of the quasi-two-parameter theory developed by Yamakawa and co-workers.[8] On the other hand, the intermolecular interaction in THF is quantified by the analyses of data of the second virial coefficient and osmotic compressibility up to considerably high concentrations, based on the scaled particle theory for wormlike spherocylinders[2] combined with the quasi-two parameter theory for the second virial coefficient.[9,10]

Dilute solution studies on CTC have already been made by many researchers so far.[11−23] We have accumulated more extensive data for the static and dynamic properties and covering a wide molecular weight range and analyzed the data on the basis of the most solid theories available, to obtain reliable molecular parameters. We will use these parameters to analyze concentrated solution properties, e.g., the isotropic-liquid crystal phase behavior, viscosity, and diffusivity, which will be discussed in forthcoming papers of this series.

† Also at CREST of Japan Science and Technology.

10.1021/ma991443u CCC: $19.00
Published on Web 03/16/2000

2. Experimental Section

Polymer Samples. CTC was synthesized by the esterification of cellulose with phenyl isocyanate. Two commercially available cellulose samples were used for the synthesis: the lower and higher molecular-weight samples were supplied by Asahi Chemical Industry Co. Ltd., Japan (Avicel), and Toyobo, Co., Ltd., Japan (cotton linters), respectively. After being purified by the method mentioned in ref 24, original cellulose samples were dried in a vacuum at room temperature and then at 60 °C for ca. 40 h.

The dried cellulose sample was mixed with pyridine, and phenyl isocyanate was added to the mixture to the amount of nine times the molar ratio to glucose units (i.e., three times that expected for full substitution). Pyridine and phenyl isocyanate were distilled over barium oxide and calcium hydrate, respectively. The mixture was heated to 110 °C for ca. 12 h under argon atmosphere and stirred by a magnetic bar to achieve complete reaction. After the reaction, the mixture became a clear brown solution. The product was precipitated into a large quantity of ethanol and collected on a glass filter. It was dissolved in acetone, filtrated through a glass filter, and reprecipitated into water. The reprecipitation was repeated twice, and after drying in a vacuum, a colorless fibrous sample was obtained.

The synthesized CTC samples were divided into fractions by fractional precipitation with acetone as the solvent and water (for low molecular weight samples) or methanol (for high molecular weight samples) as the precipitant. Fractions with similar intrinsic viscosities or elution times of GPC were combined and subjected to the further fractional precipitation. Finally middle fractions of the second generation were divided into three or four fractions by using the isotropic−cholesteric phase separation with THF as the solvent, and middle fractions (F10−F23) were used for the following physical measurements. Higher molecular weight fractions of the second generation (F1−F9) were also used for the same measurements.

The degrees of substitution of several fractions arbitrarily chosen were estimated to be 3.0 ± 0.2 from the content of the nitrogen in the samples determined by element analysis.

Static Light Scattering. Light-scattering intensities were measured for THF solutions of the above 23 CTC samples at 25 °C on a Fica 50 light-scattering photogoniometer with vertically polarized 546 nm light and without an analyzer. The photogoniometer was calibrated with benzene as the reference material.

Test solutions with the mass concentrations c lower than three times the overlap concentration[25] c^* were optically purified by the filtration through a 0.5 or 1 μm Millipore filter, followed by centrifugation at $1.7 \times 10^4 g$ for 1.5 h using a Sorvall RC5−C centrifuge. The middle portion of each solution was transferred into a cylindrical light-scattering cell with a 23 mm inner diameter, using a pipet; the cell and pipet had been rinsed with refluxing acetone vapor for 8 h in advance. The polymer concentration after centrifugation was checked to confirm that it had not changed from the original concentration.

On the other hand, test solutions with $c > 3c^*$ were prepared as follows.[25] At first, a solution with $c \approx 3c^*$ was prepared and then filtrated through a Millipore filter directly into a cylindrical cell with a 15 mm inner diameter. Then the solution in the cell was gently heated below the boiling temperature to evaporate the solvent slowly, yielding a solution with a given concentration. Finally the solution was centrifuged at $1.2 \times 10^4 g$ for 2−3 h in the Sorvall RC5−C centrifuge, and the cell was set on the photogoniometer without disturbance to measure the scattering intensity. The solvent evaporation, centrifugation, and intensity measurement were repeated to obtain the Rayleigh ratio as a function of c. The mass concentration c of a concentrated solution was calculated from the weight fraction w of the polymer in solution by the equation

$$c = \frac{w}{v_0(1 - w) + \bar{v}w} \tag{2.1}$$

where v_0 is the specific volume of the solvent and $\bar{v}$ is the partial specific volume of CTC in THF; $\bar{v}$ was determined to be 0.716 cm^3/g.

The refractive index differences between a CTC solution and solvent THF and also between two CTC solutions with different c were measured at 25 °C by a modified Schulz−Cantow type differential refractometer with 546 nm incident light. The specific refractive index increment $\partial n/\partial c$ obtained was 0.170 ± 0.02 cm^3/g irrespective of c, within the range of c examined (≈0.08 g/cm^3).

The Rayleigh ratio for the two lowest molecular weight samples (F22 and F23) was corrected for the optical anisotropy and adsorption to estimate the true weight-average molecular weight M_w and second virial coefficient A_2. The depolarized component of the scattered light was measured on a Fica 50 light-scattering photogoniometer with vertically polarized 546 nm light and a horizontally oriented analyzer, and the optically anisotropy factor δ was estimated to be 6.6×10^{-3} for sample F23 and 5.7×10^{-3} for sample F22. The adsorption coefficient ϵ of the two CTC samples in THF at 546 nm was measured by a double-beam UV−visible spectrometer (Shimadzu UV-2000); $\epsilon = 0.982$ cm^2/g for sample F23 and $\epsilon = 0.945$ cm^2/g for sample F22. Those results of δ and ϵ were used to calculate M_w and A_2 for the two CTC samples by the established method.[26] On the other hand, the effects of the optical anisotropy and adsorption were negligibly weak for the higher molecular weight CTC samples.

Dynamic Light Scattering. Dynamic light-scattering measurements were made for dilute THF solutions ($c \lesssim 6 \times 10^{-3}$ g/cm^3) of 11 CTC samples at 25 °C with an ALV/DLS/SLS-5000 light-scattering system, with an argon ion laser (NEC, GLG3110) emitting vertically polarized light of 488 nm wavelength as the light source. Test solutions were prepared by the same procedure as that applied in the static light-scattering experiment for dilute solutions, mentioned above.

Normalized autocorrelation functions $g^{(2)}(t)$ of scattered light intensity were obtained at $\theta = 20-90°$ and different c, and $g^{(2)}(t) - 1$ was semilogarithmically plotted against the time t to determine the first cumulant Γ as a function of c and the square of the scattering vector k^2. The hydrodynamic radius R_H was estimated by the equation

$$R_H = \frac{k_B T}{6\pi\eta^{(S)}} \left(\lim_{c,k^2 \to 0} \Gamma/k^2 \right)^{-1} \tag{2.2}$$

where $k_B T$ is the Boltzmann constant multiplied by the absolute temperature and $\eta^{(S)}$ is the solvent viscosity.

Viscometry. Shear viscosities of dilute THF solutions of 20 CTC samples were measured at 25 °C by a low-shear four-bulb capillary viscometer (samples F1 and F2) or a conventional Ubbelohde-type capillary viscometer (the other samples). The intrinsic viscosity $[\eta]$ and the Huggins coefficient k' of each CTC sample were determined from Huggins and Mead−Fuoss plots.

3. Results

Molecular Weight, Second Virial Coefficient, and Radius of Gyration. Figure 1 shows the plots of Kc/R_0 against c and of $(Kc/R_0)^{1/2}$ against c for dilute and semidilute THF solutions of seven relatively low molecular weight CTC samples at 25 °C obtained by static light scattering. Here K is the optical constant, c is the polymer mass concentration, and R_0 is the excess Rayleigh ratio of the solution over that of the solvent at the zero scattering angle. The linearity of the Zimm plot (the left panel) seems better than that of the Berry plot (the right panel) for higher molecular weight samples. It is known that the $(Kc/R_0)^{1/2}$ vs c plot is more linear for flexible polymers in good solvents but the opposite for solutions of a semiflexible polymer, poly(hexyl isocyanate).[27] The concentration dependence of Kc/R_0 for CTC solutions resembles that of the latter

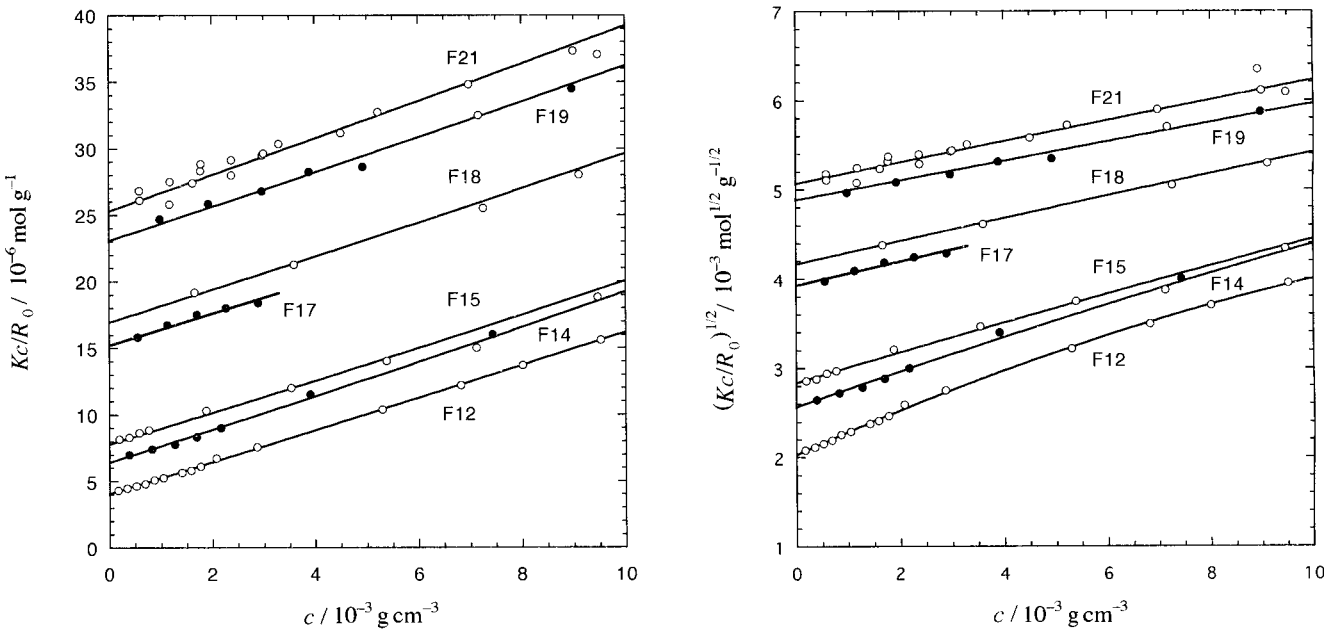

Figure 1. Concentration dependences of Kc/R_0 and $(Kc/R_0)^{1/2}$ for dilute and semidilute THF solutions of seven relatively low molecular weight CTC samples at 25 °C.

Table 1. Results of Light Scattering, Viscometry, and GPC for Cellulose Tris(phenyl carbamate) Samples

sample	$M_w/10^4$	A_2 [a]	$\langle S^2\rangle_z^{1/2}$/nm	$[\eta]$[b]	k'	R_H/nm	M_w/M_n	M_z/M_w	DS[c]
F1	392	3.49	123	13.6	0.41	87.0			
F2	382	3.79	131	13.6	0.44				
F3	262	3.73	103	10.6	0.43				
F4	240	3.97	105	10.6	0.40	65.4			
F5	177	4.35	84.8	8.14	0.41	52.1			
F6	111	3.97	70.4			42.8			
F7	108	4.01	70.1	5.63	0.38	44.8			
F8	91.0	3.99	62.0	5.33	0.40				
F9	55.5	4.44	44.4	3.35	0.37				
F10	53.4	3.81	41.2	2.84	0.40	26.3			
F11	33.9	4.98	32.0	2.14	0.38		1.10	1.09	
F12	23.2	5.23	28.2	1.77	0.37	16.1	1.07		3.1
F13	15.6	5.03	21.4	1.20	0.37		1.07	1.06	
F14	15.0	5.37	20.9	1.19	0.35	12.2	1.05		3.0
F15	12.7	5.63	19.1						
F16	10.3	5.02	16.5	0.834	0.36		1.08	1.06	
F17	6.42	5.37		0.483	0.39	6.94			
F18	5.87	5.97		0.481	0.41		1.07	1.06	3.2
F19	4.06	5.47		0.318	0.42	5.42	1.08		2.8
F20	3.94	5.64		0.339	0.39		1.06	1.05	
F21	3.87	6.41							
F22	2.51	6.20		0.202	0.45				
F23	1.91	6.18		0.145	0.46	3.33			3.0

[a] In units of 10^{-4} cm^3 g^{-1}mol. [b] In units of 10^2 cm^3 g^{-1}. [c] Degree of substitution.

polymer solutions. The weight-average molecular weight M_w and the second virial coefficient A_2 were estimated from the intercept and initial slope of the Zimm plot for all the samples examined. The results are listed in Table 1. The analysis by the Berry plot provides almost the identical M_w but a ca. 20% larger A_2.

The molecular weight dependence of A_2 is shown in Figure 2 by unfilled circles along with the results of Daňhelka et al.[23] for the same system (small dots). Our data points follow a curve with a slightly negative slope (≈ -0.1). This molecular weight dependence of A_2 is appreciably weaker than that for flexible polymers in good solvents ($A_2 \propto M^{-\delta}$ with δ usually found in the range 0.2−0.3[28]).

Figure 3 shows plots of the intramolecular interference factor $P(\theta)$ against the square of the scattering vector k^2 for chosen 6 CTC samples. The z-average radius of gyration $\langle S^2\rangle_z^{1/2}$ of each sample was determined from the initial slope of the plot. The results of $\langle S^2\rangle_z^{1/2}$ for 16 CTC samples are listed in Table 1, and the molecular weight dependence of $\langle S^2\rangle_z^{1/2}$ is shown by unfilled circles in Figure 4, along with Daňhelka et al.'s results[23] (small dots) for the same system. Our and Daňhelka et al.'s data follow a common curve with the slopes 0.70 (±0.02) at $M_w \lesssim 3 \times 10^5$ and 0.55 (±0.02) at $M_w \gtrsim 1 \times 10^6$. The former slope indicates the stiffness of the CTC chain.

Hydrodynamic Radius and Intrinsic Viscosity. Figure 5 shows the autocorrelation function $g^{(2)}(t)$ for sample F12 at $c = 1.124 \times 10^{-3}$ g/cm^3, as an example. Here, the abscissa is the time t in the correlation function multiplied by the square of the scattering vector k^2. The data points at $\theta = 20-90$ ° nicely follow straight lines within the k^2t range shown, except at very

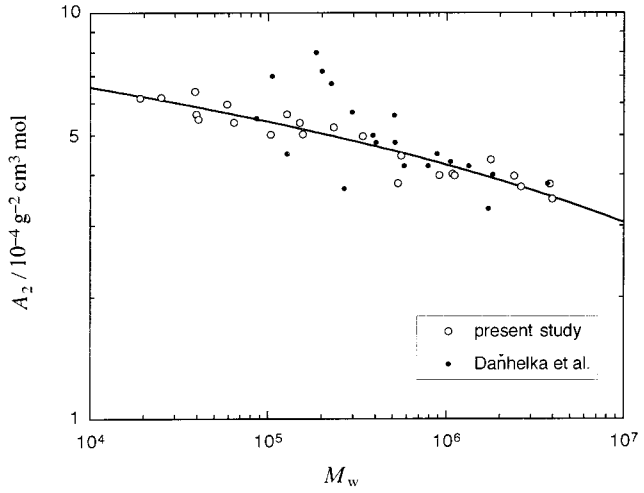

Figure 2. Molecular weight dependence of A_2 for CTC in THF in 25 °C. Key: unfilled circles, the present data; small dots, the results of Daňhelka et al.[23]

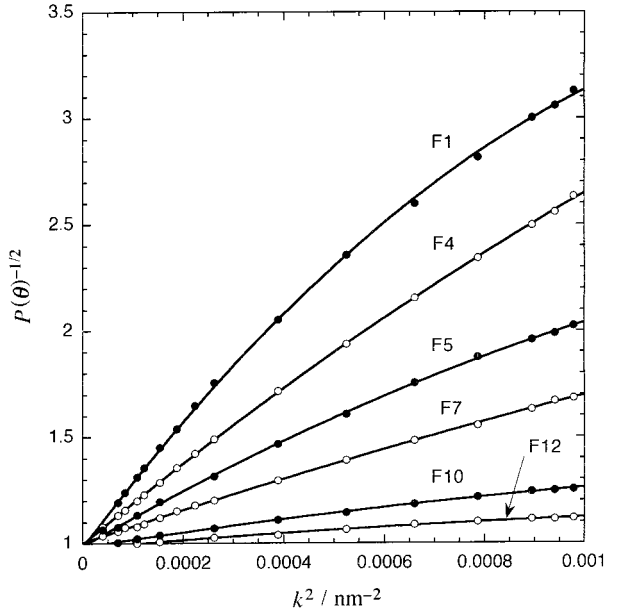

Figure 3. Intramolecular interference factor $P(\theta)$ for chosen 6 CTC samples in 25 °C THF.

small k^2t. The upward deviation at small k^2t is more remarkable at higher θ, which may relate to some fast local motions of the polymer chain. (Similar upward deviations in $g^{(2)}(t)$ were sometimes reported for other polymer solutions.[29]) Here we neglected the data points at such a small k^2t to estimate the first cumulant Γ. The straight lines for different θ shown in Figure 5 have almost identical slopes, which mean that Γ/k^2 is almost independent of k^2. The hydrodynamic radius R_H was estimated from Γ/k^2 values using eq 2.2.

The values of R_H for other CTC samples were obtained in a similar way. It is noted that for high molecular weight samples, the linear region in the plot of ln $[g^{(2)}(t) - 1]$ vs t becomes narrower, and Γ/k^2 becomes an increasing function of k^2. All the results of R_H are listed in Table 1. The molecular weight dependence of R_H was well expressed by

$$R_H/\text{nm} = (8 \mp 1.5) \times 10^{-3} M_w^{0.61_5 \pm 0.01_5} \quad (3.1)$$

The molecular weight dependence of the intrinsic viscosity $[\eta]$ is shown in Figure 6. The data points

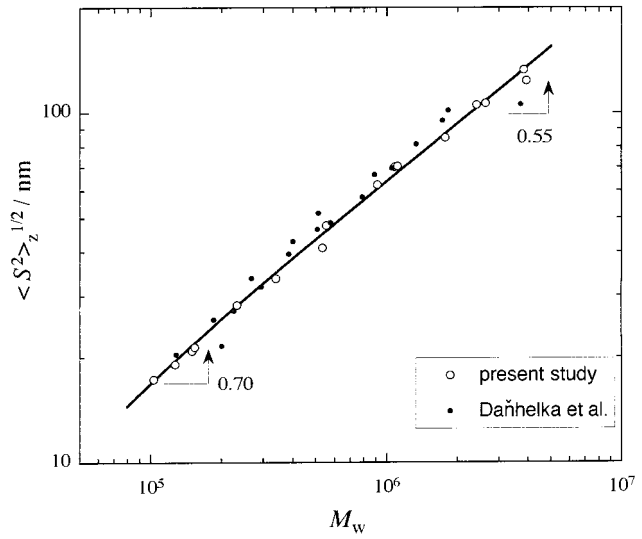

Figure 4. Molecular weight dependence of $\langle S^2 \rangle_z^{1/2}$ for CTC in THF at 25 °C. Key: unfilled circles, the present data; small dots, the results of Daňhelka et al.[23]

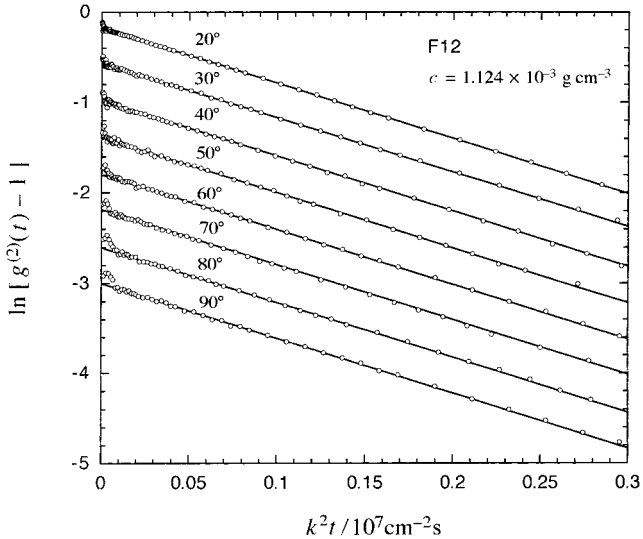

Figure 5. Plots of $\ln[g^{(2)}(t) - 1]$ against k^2t for a THF solution of sample F12 with $c = 1.124 \times 10^{-3}$ g/cm^3. Data points at each θ (except at 20°) are shifted downward for viewing clarity.

(unfilled circles) follow a curve with the slope of 0.98 (±0.05) at $M_w \lesssim 1 \times 10^5$ and 0.74 (±0.04) at $M_w \gtrsim 1 \times 10^6$. The former slope indicates that CTC is a semiflexible polymer. In Figure 6, $[\eta]$ data of Daňhelka et al.[23] for the same system are shown by small dots. Their results show almost the same molecular weight dependence of $[\eta]$ as ours except at low M_w, where their data points slightly deviate upward from our experimental curve.

Osmotic Compressibility. Figure 7 plots Kc/R_0 against c for dilute through concentrated THF solutions of six CTC samples examined. As demonstrated in Figure 1, Kc/R_0 is proportional to c up to $c \approx 1 \times 10^{-2}$ g/cm^3, but the data points follow curves concave upward in a wider c range shown in Figure 7. This indicates that the third and higher virial terms are significant at $c \gtrsim 1 \times 10^{-2}$ g/cm^3. Since the plot of $(Kc/R_0)^{1/2}$ vs c has a downward curvature (cf. Figure 1), the higher virial terms relative to the second virial term for CTC in THF are smaller than the case of flexible polymers in good solvents.[30] This is a characteristic feature of stiff−polymer solutions.[25]

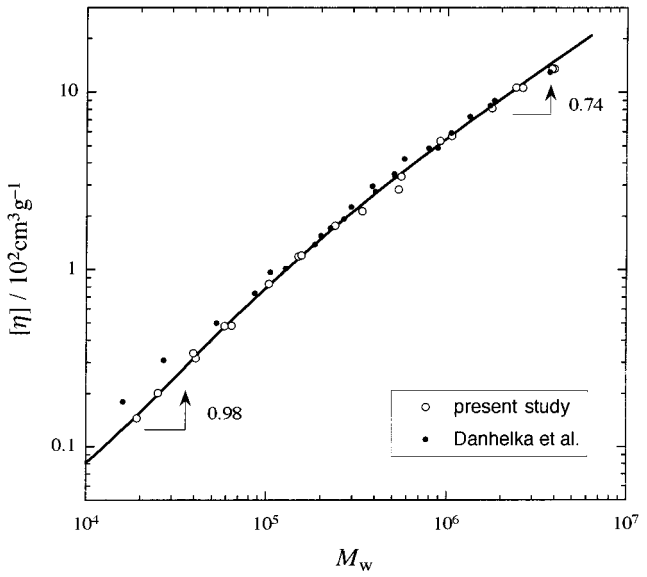

Figure 6. Molecular weight dependence of $[\eta]$ for CTC in THF at 25 °C. Key: unfilled circles, the present data; small dots, the results of Daňhelka et al.[23]

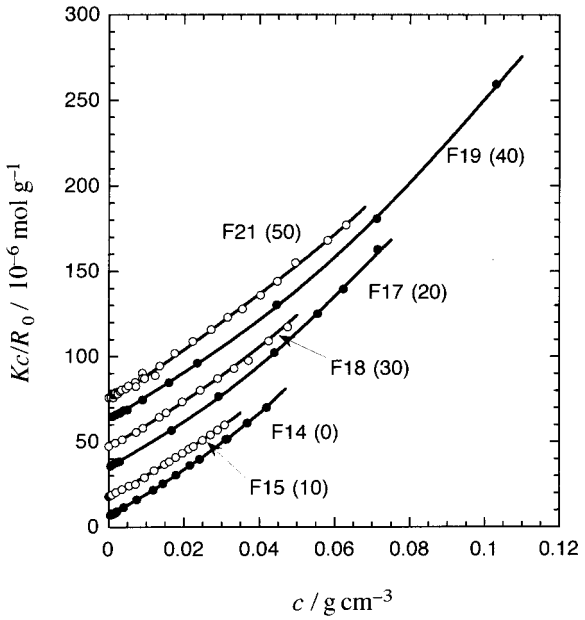

Figure 7. Concentration dependence of Kc/R_0 for dilute through concentrated THF solutions of six CTC samples (25 °C). The theoretical curve and experimental data points for each sample (except for sample F14) are shifted upward by the amount indicated in parentheses.

From the fluctuation theory of light scattering, the excess Rayleigh ratio R_0 of a solution of monodisperse polymer at the zero scattering angle is related to the osmotic compressibility $\partial c/\partial\Pi$ of the solution by

$$R_0/Kc = RT\partial c/\partial\Pi \tag{3.2}$$

where RT is the gas constant multiplied by the absolute temperature. As shown above, our CTC samples are reasonably narrow in molecular weight distribution, though not monodisperse. Therefore, the data of Kc/R_0 in Figure 7 will be analyzed by using eq 3.2 in section 4.

4. Discussion

Determination of the Wormlike-Chain Parameters. According to Benoit and Doty,[31] the mean-square radius of gyration $\langle S^2\rangle$ of the unperturbed wormlike chain of molecular weight M can be written as

$$\langle S^2\rangle = (2q)^2\left[\frac{1}{6}N-\frac{1}{4}+\frac{1}{4N}-\frac{1}{8N^2}(1-e^{-2N})\right] \tag{4.1}$$

where q is the persistence length and N is the Kuhn statistical segment number defined by $N \equiv M/2qM_L$ with M_L the molar mass per unit contour length. If N is larger than 2, eq 4.1 can be approximated by[27]

$$\left(\frac{M}{\langle S^2\rangle}\right)^{1/2} = \left(\frac{3M_L}{q}\right)^{1/2}\left(1+\frac{3qM_L}{2M}\right) \tag{4.2}$$

This equation indicates that the wormlike-chain parameters q and M_L may be estimated from the intercept and slope of the plot of $(M_w/\langle S^2\rangle_z)^{1/2}$ vs $1/M_w$ constructed from experimental data of $\langle S^2\rangle_z$ and M_w, if $\langle S^2\rangle_z$ is free from the intramolecular excluded-volume effect. (The effect of polydispersity in molecular weight will be considered later.)

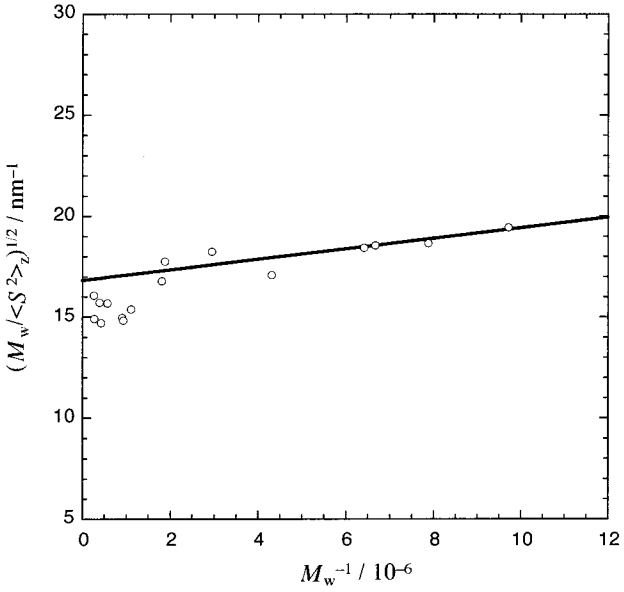

Figure 8. Plots of $(M_w/\langle S^2\rangle_z)^{1/2}$ against $1/M_w$ constructed from our experimental data shown in Figure 4.

In Figure 8, $(M_w/\langle S^2\rangle_z)^{1/2}$ calculated from our experimental data of CTC are plotted against $1/M_w$. Although slightly scattered, data points follow the indicated straight line at $1/M_w > 1.8 \times 10^{-6}$. From the intercept and slope of this line, q and M_L were estimated to be $10._5$ ($\pm$1) nm and 990 ($\pm$70) nm^{-1}, respectively, using eq 4.2. It turns out that N of all the samples plotted in Figure 8, calculated from the above q and M_L values, are larger than 5, fulfilling the condition of the validity of eq 4.2. The downward deviations of the data points at $1/M_w < 1.1 \times 10^{-6}$ from the indicated line may be due to the intramolecular excluded-volume effect on the CTC chain as will be discussed below.

Yamakawa and co-workers[8,9,32,33] developed a theory of the intramolecular excluded-volume effect of the polymer chain on the basis of the helical wormlike chain, which includes the wormlike chain as a special case. According to their theory, the radius expansion factor α_S due to the excluded-volume effect can be calculated as a known function (cf. eq 8.57 in ref 8 or eq 42 in ref 33) of the scaled excluded-volume parameter $\tilde{z}$ defined by

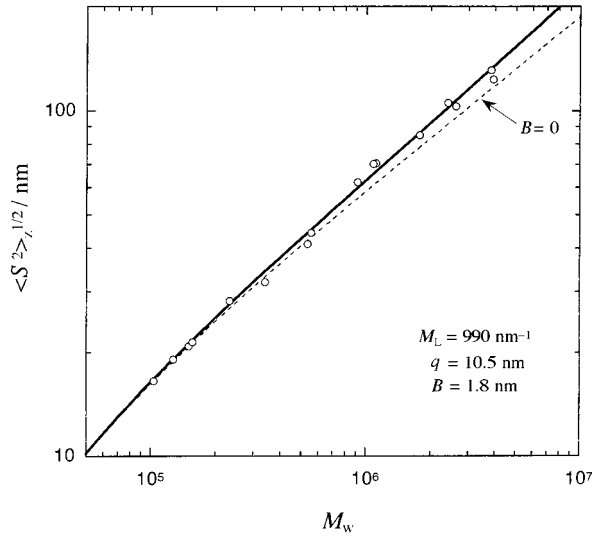

Figure 9. Comparison between our $\langle S^2\rangle_z$ data and the theoretical values (solid curve) calculated by the quasi-two parameter theory for the wormlike chain with $q = 10._5$ nm, $M_L = 990$ nm^{-1}, and $B = 1.8$ nm. Dashed curve: theoretical values for $B = 0$.

$$\tilde{z} \equiv \frac{3}{4}K(N)\cdot\left(\frac{3}{2\pi}\right)^{3/2}\frac{B}{2q}N^{1/2} \qquad (4.3)$$

where $K(N)$ is a known function of N (cf. eq 8.46 in ref 8 or eq 50 in ref 33) and B is the excluded-volume strength with the unit of length.

Combining Yamakawa et al.'s theory with eq 4.1, we can calculate the radius of gyration of the wormlike chain perturbed by the excluded-volume effect. In Yamakawa et al.'s theory, B is an unknown parameter, and we sought a value of B to fit the theoretical $\langle S^2\rangle$ to experimental $\langle S^2\rangle_z$ of CTC. Figure 9 compares our $\langle S^2\rangle_z$ data with the theoretical values, when q, M_L, and B are chosen to be $10._5$ nm, 990 nm^{-1}, and 1.8 nm, respectively. The theoretical solid curve closely fit the data points over the entire molecular weight range studied. When q and M_L were allowed to vary within the ranges of uncertainties mentioned above, B changed from 1.7 to 1.9 nm.

As is known, the analysis of $\langle S^2\rangle_z$ for polydisperse samples by eq 4.1 or eq 4.2 gives a value of M_L which is smaller than the true value. If $N \gtrsim 5$, this polydispersity effect may be corrected by multiplying M_L by M_z/M_w (M_z: the z-average molecular weight).[24] Since GPC measurements gave a value around 1.06 for M_z/M_w of our CTC samples (cf. Table 1), the corrected M_L becomes 1050 ($\pm$70) nm^{-1}.

Data of $[\eta]$ and R_H can be analyzed in a similar way. While $[\eta]$ and R_H of wormlike cylinders in the unperturbed state are calculated by the theory of Yamakawa, Fujii, and Yoshizaki,[34−37] the expansion factors α_η and α_H for $[\eta]$ and R_H, respectively, are calculated from $\tilde{z}$ according to Yamakawa et al.[9,32,33] [cf. eq 8.69 in ref 8 or eq 13 in ref 47 for α_η and eqs 8.65, 8.70, and 8.74 in ref 8 or eqs 8 and 10−12 ($d/a = 1$) in ref 47 for α_H]. The necessary parameters for such calculations are q, M_L, B and the diameter d of the wormlike cylinder. Here, we have assumed the values of q and B to be the same as those determined by the radius of gyration data and have taken M_L and d as adjustable parameters. Figures 10 and 11 show the fitting results of $[\eta]$ and R_H as well as the wormlike-cylinder parameters chosen. The agreements between theory and experiment are

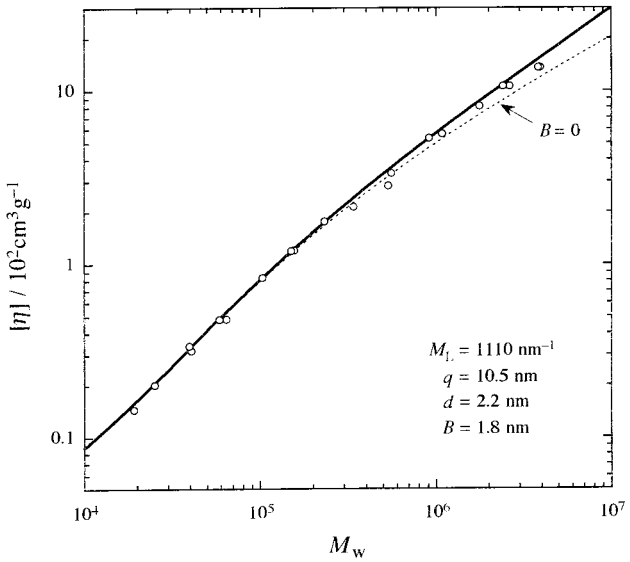

Figure 10. Comparison between our $[\eta]$ data and the theoretical values (solid curve) calculated by the quasi-two parameter theory for the wormlike chain with $q = 10._5$ nm, $M_L = 1110$ nm^{-1}, $B = 1.8$ nm, and $d = 2.2$ nm. Dashed curve: theoretical values for $B = 0$.

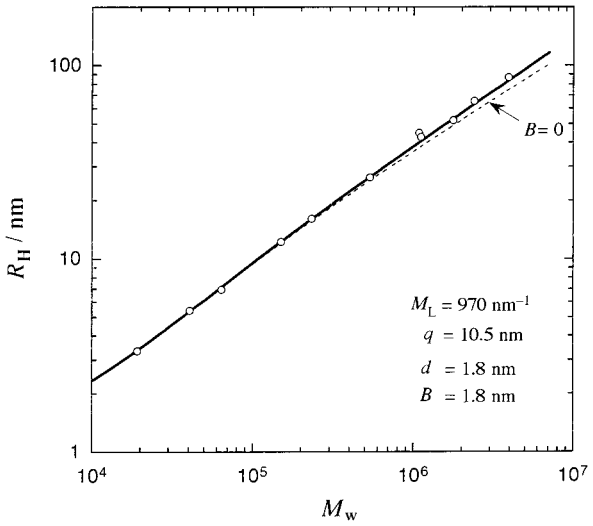

Figure 11. Comparison between the measured R_H and the theoretical values (solid curve) calculated by the quasi-two parameter theory for the wormlike chain with $q = 10._5$ nm, $M_L = 970$ nm^{-1}, $d = 1.8$ nm, and $B = 1.8$ nm. Dashed curve: theoretical values for $B = 0$.

satisfactory in both figures. The uncertainties in q and B determined from the radius of gyration data slightly changed the best-fit values of M_L and d, as shown in Table 2. Polydispersity effects on $[\eta]$ and R_H are known to be much weaker than that on $\langle S^2\rangle_z$, so that the values of M_L estimated from $[\eta]$ and R_H are little affected by the effects.

The dashed curves in Figures 9−11 indicate the theoretical values of $\langle S^2\rangle$, $[\eta]$, and R_H for an unperturbed wormlike chain with $B = 0$. Appreciable deviations of the experimental data points from the dashed curvesare observed at $M_w \gtrsim 10^6$ in all of the figures, indicating that the excluded-volume effect becomes appreciable above such M_w for CTC in THF. This critical molecular weight corresponds to $N = 50$, which agrees with the critical N for the onset of the excluded-volume effect, observed for other stiff or semiflexible polymer solutions.[1,48] In Figure 11, it can be seen that the apparent

Table 2. Parameters Characterizing the Conformation and Intermolecular Interaction of CTC in THF (25 °C)

method	M_L/nm^{-1}	q/nm	B/nm	d/nm	d_0/nm	δ/nm	δ'/nm	δ''/nm
$\langle S^2\rangle$	990 ± 70 (1050 ± 70[a])	$10._5 \pm 1$	1.8 ± 0.1					
$[\eta]$	1110 ± 60	$10._5 \pm 1$[b]	1.8 ± 0.1[b]	2.2 ± 0.3				
R_H	970 ± 70	$10._5 \pm 1$[b]	1.8 ± 0.1[b]	1.8 ± 0.2				
A_2 and $\partial\Pi/\partial c$			$2.1_5 \pm 0.3$		1.4 ± 0.1	−0.1 ± 0.1	−1.5	0[b]
X-ray[c] [38]	1020				1.66			
$\bar{v}$					1.26[d]			

[a] Value corrected with respect to polydispersity in molecular weight (see text). [b] Assumed value. [c] For a single crystal of the CTC−methyl ethyl ketone complex. [d] Diameter d_v calculated from the partial specific volume $\bar{v}$ by eq 4.12.

power law relation between R_H and M_w (cf. eq 3.1) comes from the combination of the chain-stiffness effect and the excluded-volume effect.

Table 2 summarizes the values of M_L determined from $\langle S^2\rangle$, $[\eta]$, and R_H. The M_L value determined from $[\eta]$ is somewhat larger than that from R_H. The same trend was observed for some flexible polymers, and Yamakawa pointed out that it may come from the preaveraged approximation of the Oseen tensor used at the hydrodynamic calculation.[8] The M_L value determined by $\langle S^2\rangle$ is intermediate between those from $[\eta]$ and R_H, and we obtain a value of 1040 (±70) nm^{-1} for M_L of CTC on average, which is close to those reported previously by Daňhelka et al.[23] This value along with the molar mass 519 per glucose residue of CTC yield 0.50 (±0.03) nm for the projection length of the residue along the CTC chain contour. This length is favorably compared with the pitch 0.508 nm per residue of the $^3/_2$ helix of CTC in the crystalline state of the CTC-methyl ethyl ketone complex proposed by Zugenmaier and Vogt,[38] so that the *local* conformation of the CTC chain in solution may be the same as that in the crystalline state.

Values of q of CTC reported so far range from 3 to 13 nm in different solvent conditions.[11,23,39,16,40] In general, q of CTC is reduced with increasing the temperature. Our result of q of CTC in THF at 25 °C is close to that (=9.7 nm) determined by Daňhelka et al.[23] under the same solvent conditions and also those in acetone,[11,23] dioxane,[11,41] pyridine,[11] and in 1-methyl-2-pyrrolidone (NMP)[39] at 20 or 25 °C but is much larger than those in benzophenone,[16] cyclohexanol,[40] and anisol[40] at 70−90 °C (cf. Table 3 in ref 23)).

Reported values of q for other cellulose derivatives are in a similar range. Although q of cellulose trinitrate in acetone at 20 °C is slightly large (17 nm),[42] reported q values at 25 °C are 7.8 nm for cellulose tris(3,5-dimethylphenyl carbamate) in NMP,[24,5] 6.7 nm for (acetoxypropyl)cellulose in dimethyl phthalate,[43] 6.5 nm for (hydroxypropyl)cellulose in dimethylacetamide,[44] and 5.3 nm for cellulose triacetate in trifluoroacetic acid.[45,46]

Determination of the Intermolecular Interaction Parameters. Yamakawa and Stockmayer[9] and Yamakawa[10] formulated the second virial coefficient A_2 on the basis of the touched-bead model of the wormlike chain. Including effects of chain ends, the theory expresses A_2 in the form

$$A_2 = \frac{N_A B}{2M_L^2} h(\hat{z}) + \frac{a_{2,1}}{M} + \frac{a_{2,2}}{M^2} \tag{4.4}$$

where N_A is the Avogadro constant and $h(\hat{z})$ is the function

$$h(\hat{z}) = (1 + 7.74\hat{z} + 52.3\hat{z}^{27/10})^{-10/27} \tag{4.5}$$

of the parameter $\hat{z}$ defined by

$$\hat{z} \equiv \frac{Q(N, d_b/2q)}{2.865} \cdot \left(\frac{3}{2\pi}\right)^{3/2} \frac{BN^{1/2}}{2q\alpha_S^3} \tag{4.6}$$

with Q a function of N and $d_b/2q$ (d_b: the bead diameter), and α_S the radius expansion factor. While α_S is calculated from $\tilde{z}$ (see above), Q (for $N > 1$) is calculated by eqs 96 and 119 of ref 9. Furthermore, $a_{2,1}$ and $a_{2,2}$ are associated with interactions between intermediate and chain-end beads and between two chain-end beads, respectively.

If the molecular weight M is high enough, we may neglect the second and third terms in eq 4.4. To calculate the leading term in this equation, we need the parameters, M_L, q, d_b, and B. Since the Q function is insensitive to the value of d_b, it may be approximated by the average of d (2 nm) determined from $[\eta]$ and R_H mentioned above. Although the other three parameters were also determined above, we took B as an adjustable parameter to compare eq 4.4 without the second and third terms, with A_2 data of CTC in THF (cf. Figure 2). With M_L and q fixed, respectively, to be 1040 (±70) nm^{-1} and 10.5 (±1) nm, the best fit of our A_2 data (except at very low M_w) to eq 4.4 without the second and third terms was obtained when B was chosen to be 2.1_5 (±0.3) nm (cf. Figure 12). Upward deviations of the data points from the solid curve in Figure 12 at $M_w > 1 \times 10^5$ may be due to effects of chain ends (see below). The value of B is slightly larger than that [1.8 (±0.1) nm] determined from $\langle S^2\rangle$, but this difference in B does not essentially change the theoretical curves for $\langle S^2\rangle$, $[\eta]$, and R_H shown in Figures 9−11 due to weakness of the intramolecular excluded-volume effect for the CTC chain.

The second virial coefficient A_2 can be also calculated for the wormlike spherocylinder model, provided the polymer chain is so stiff that it cannot contact with another polymer chain simultaneously at two or more portions along the chains.[2] (This condition for the wormlike spherocylinder should be distinguished from the single-contact condition for the bead model. For the bead model, multiple-contacts in two chains at a short range along the chain contours is always important when the two chain contours are locally parallel each other.[9] On the other hand, for the cylinder model such short-range multiple contacts *are regarded as a single contact*.) Including effects of chain ends, we have

$$A_2 = \frac{\pi d_0 N_A}{4M_L^2}\left[1 + \frac{\delta}{d_0} + \left(\frac{8}{3} + \frac{\delta'}{d_0}\right)\frac{d_0 M_L}{M} + \left(\frac{4}{9} + \frac{\delta''}{d_0}\right)\left(\frac{d_0 M_L}{M}\right)^2\right] \tag{4.7}$$

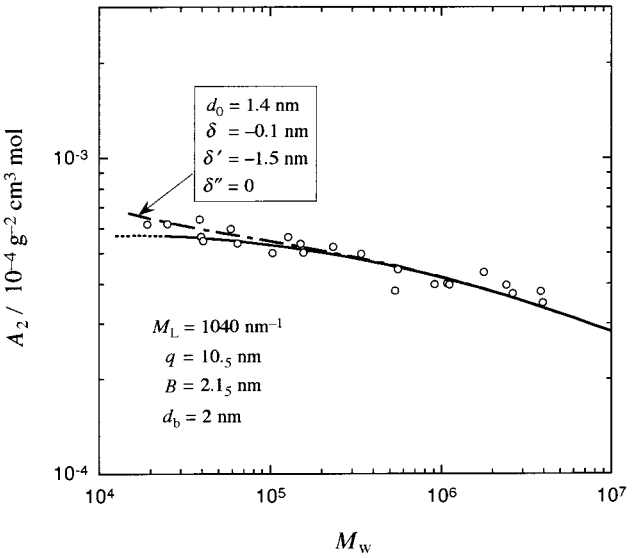

Figure 12. Comparison between our A_2 data and the theoretical values (solid curve) calculated by the quasi-two parameter theory for the wormlike chain (eq 4.4) with $q = 10.5$ nm, $M_L = 1040$ nm^{-1}, $d_b = 2.0$ nm, $B = 2.15$ nm, and $a_{2,1} = a_{2,2} = 0$ (dotted curve, the extrapolation of the theoretical curve to $N < 1$). Dot−dash curve: theoretical values including effects of chain ends with eq 4.9 with $d_0 = 1.4$ nm, $\delta = -0.1$ nm, $\delta' = -1.5$ nm, and $\delta'' = 0$.

where d_0 is the hard-core diameter of the wormlike spherocylinder and δ, δ', and δ'' are related to the strengths of the soft dispersion interaction between middle portions, middle and end portions, and two end portions of two wormlike spherocylinders, respectively. When the dispersion interaction is attractive, the values of δ, δ', and δ'' are negative.[2] This equation should become identical with eq 4.4 at $N \to 0$, so that we have the relations

$$d_0 + \delta = (2/\pi)Bh_0(\hat{z}) \tag{4.8}$$

and

$$a_{2,1} = \frac{\pi d_0 N_A}{4M_L}\left(\frac{8}{3}d_0 + \delta'\right),\ a_{2,2} = \frac{\pi {d_0}^2 N_A}{4}\left(\frac{4}{9}d_0 + \delta''\right) \tag{4.9}$$

where $h_0(\hat{z})$ is $h(\hat{z})$ at $N \to 0$. As pointed out by Yamakawa and Stockmayer,[9] multiple-contact terms are important even in the rod limit ($N \to 0$) for the bead model. The quantity $1 - h_0(\hat{z})$ represents the contributions to A_2 of the double and more contacts relative to that of the single contact for the bead model in the rod limit.

Unfortunately, the Q function at $N < 1$ is not known, but we may evaluate $h_0(\hat{z})$ by naturally extrapolating the plot of $h(\hat{z})$ vs N toward $N \to 0$. For CTC in THF, this extrapolation gives $h_0(\hat{z}) = 0.96$, and with eq 4.8, we obtain the relation $d_0 + \delta = 1.3$ (±0.2) nm for the wormlike spherocylinder parameters.

For the wormlike spherocylinder model, the osmotic compressibility is formulated using the scaled particle theory (SPT) with the "single-contact approximation." Incorporating a soft attractive (dispersion) interaction into the SPT in a perturbative way, we can write $\partial\Pi/\partial c$ (the inverse of the osmotic compressibility) in the isotropic state as[2]

$$\frac{\partial\Pi}{\partial c} = \frac{RT}{M(1-\upsilon c')^2}\left[1+B_I\frac{c'}{1-\upsilon c'} + 2C_I\left(\frac{c'}{1-\upsilon c'}\right)^2\right] + \frac{\pi N_A}{2{M_L}^2}\left[\delta+\delta'\frac{d_0 M_L}{M} + \delta''\left(\frac{d_0 M_L}{M}\right)^2\right]c \tag{4.10}$$

where M and c' are the molecular weight and the number concentration ($=cN_A/M$) of the spherocylinder, respectively, and υ, B_I, and C_I are defined by

$$\upsilon \equiv \frac{\pi}{4}L_c{d_0}^2 + \frac{\pi}{6}{d_0}^3,\quad B_I \equiv \frac{\pi}{2}{L_c}^2 d_0 + 6\upsilon,$$
$$C_I \equiv \left(\upsilon + \frac{\pi}{12}{d_0}^3\right)\left(B - 2\upsilon - \frac{\pi}{6}{d_0}^3\right) \tag{4.11}$$

with L_c the contour length of the cylinder part of the spherocylinder ($=M/M_L - d_0$).

For given values of the interaction parameters, d_0, δ, δ', and δ'', we can calculate A_2 and $\partial\Pi/\partial c$ including the chain-end effect with eqs 4.4, 4.9, and 4.10, where B in eq 4.4 is related to d_0 and δ by eq 4.8. Equation 4.4 for A_2 considers the effect of multiple contacts, but eq 4.10 for $\partial\Pi/\partial c$ does not. Since the solid curve in Figure 12 is almost horizontal at $M_w \lesssim 2 \times 10^5$, the effect of multiple contacts may not be appreciable at such M_w. Thus, we compare eq 4.10 with experimental data of $\partial\Pi/\partial c$ for CTC samples with $M_w < 2 \times 10^5$. Among the four interaction parameters, $d_0 + \delta$ must be fixed to be 1.3 (±0.2) nm as mentioned above. Furthermore, since effects of polymer chain ends are weak for CTC in THF as seen from the comparison between the solid curve and experimental data at low M_w in Figure 12, we simply omit the terms of δ'' in eqs 4.9 and 4.10.

A trial and error method was used to find values of d_0 and δ' which lead to the closest agreements between A_2 data and eq 4.4 and between $\partial\Pi/\partial c$ data at $M_w \lesssim 2 \times 10^5$ and eq 4.10 under the condition $d_0 + \delta = 1.3$ (±0.2) nm. As shown in Figures 12 and 13, eqs 4.4 and 4.10 with $d_0 = 1.4$ (±0.1) nm and $\delta' = -1.5$ nm give the best fits to the data points for both A_2 and $\partial\Pi/\partial c$. The value of δ is calculated to be −0.1 (±0.1) nm from $d_0 = 1.4$ (±0.1) nm, and this indicates that the attractive interaction of CTC is weak in THF and CTC chains interact each other mainly by the hard-core repulsion in THF. The value of δ' is negative, so that the dispersion interaction between the middle and end portions of CTC chains is also attractive in THF.

The X-ray diffraction study of Zugenmaier and Vogt[38] indicates that the interchain distance of CTC in crystalline state of the CTC and methyl ethyl ketone (MEK) complex is 1.66 nm. This value is slightly larger than d_0 estimated above from A_2 and $\partial\Pi/\partial c$ data. In the crystal studied by Zugenmaier and Vogt, four MEK molecules are present per monomeric unit of the CTC chain, and those solvated MEK molecules may enlarge the interchain spacing of CTC.

A diameter d_v can be estimated from the partial specific volume $\bar{v}$ by the equation

$$d_v = (4M_L\bar{v}/\pi N_A)^{1/2} \tag{4.12}$$

For CTC in THF, $\bar{v}$ is 0.716 cm^3/g, and d_v is estimated to be 1.26 nm. This diameter may be associated with the volume of solvent excluded when a polymer chain is dissolved in the solvent, and it is slightly smaller than d_0, the distance of the closest approach of two polymer chains. The hydrodynamic diameter d (≈ 2 nm) esti-

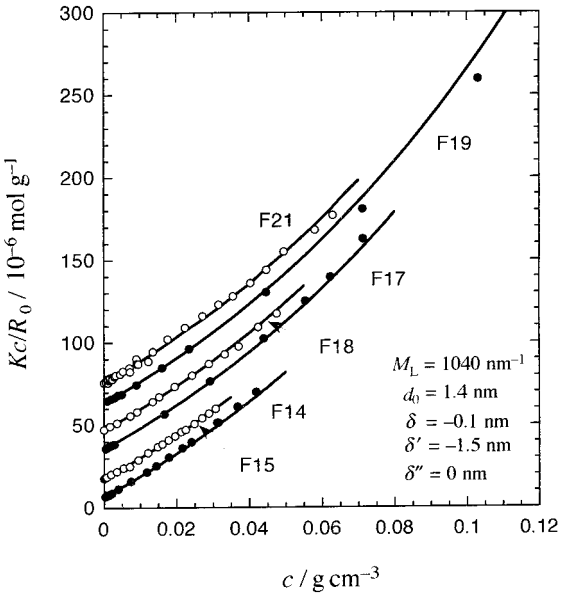

Figure 13. Comparison between the measured Kc/R_0 data with $M_w < 2 \times 10^5$ and the theoretical values (solid curve) calculated by eqs 4.10 and 4.11 (the scaled particle theory for the wormlike chain considering the soft dispersion interaction) with $M_L = 1040$ nm^{-1}, $d_0 = 1.4$ nm, $\delta = -0.1$ nm, $\delta' = -1.5$ nm, and $\delta'' = 0$. The theoretical curve and experimental data points for each sample (except for sample F14) are shifted upward to the same amount as in Figure 7 for viewing clarity.

mated above from $[\eta]$ and R_H data is larger than d_0 and also the interchain spacing in the crystalline state. Similar disagreements between d and d_0 are reported also for other stiff-chain polymers.[3]

Acknowledgment. The authors wish to thank Professor T. Norisuye at Osaka University for valuable comments and discussion.

References and Notes

(1) Norisuye, T.; Fujita, H. *Polym. J.* **1982**, *14*, 143.
(2) Sato, T.; Jinbo, Y.; Teramoto, A. *Macromolecules* **1997**, *30*, 590.
(3) Sato, T.; Teramoto, A. *Adv. Polym. Sci.* **1996**, *126*, 85.
(4) Werbowyj, R. S.; Gray, D. G. *Mol. Cryst. Liq. Cryst. (Lett.)* **1976**, *34*, 97.
(5) Tsuboi, A.; Norisuye, T.; Teramoto, A. *Macromolecules* **1996**, *29*, 3597.
(6) Kurata, M.; Stockmayer, W. H. *Fortschr. Hochpolym.-Forsch.* **1963**, *3*, 196.
(7) Flory, P. J. *Makromol. Chem.* **1966**, *98*, 128.
(8) Yamakawa, H. *Helical Wormlike Chains in Polymer Solutions*; Springer-Verlag: Berlin & Heidelberg, Germany, 1997.
(9) Yamakawa, H.; Stockmayer, W. H. *J. Chem. Phys.* **1972**, *57*, 2843.
(10) Yamakawa, H. *Macromolecules* **1992**, *25*, 1912.
(11) Burchard, W.; Husemann, E. *Makromol. Chem.* **1961**, *44–46*, 358.
(12) Shanbhag, V. P. *Ark. Kem.* **1968**, *29*, 1.
(13) Shanbhag, V. P. *Ark. Kem.* **1968**, *29*, 33.
(14) Shanbhag, V. P. *Ark. Kem.* **1968**, *29*, 139.
(15) Öhman, J. *Ark. Kem.* **1969**, *31*, 125.
(16) Janeschitz-Kriegl, H.; Burchard, W. *J. Polym. Sci: Part A-2* **1968**, *6*, 1953.
(17) Burchard, W. *Br. Polym. J.* **1971**, *3*, 214.
(18) Guthrie, J. T.; Huglin, M. B.; Richards, R. W.; Shah, V. I.; Simpson, A. H. *Eur. Polym. J.* **1975**, *11*, 527.
(19) Noordermeer, J. W. M.; Daryanani, R.; Janeschitz-Kriegl, H. *Polymer* **1975**, *16*, 359.
(20) Gupta, A. K.; Marchal, E.; Burchard, W. *Macromolecules* **1975**, *8*, 843.
(21) Sutter, W.; Burchard, W. *Makromol. Chem.* **1978**, *179*, 1961.
(22) Fried, F.; Searby, G. M.; Seurin-Vellutini, M. J.; Dayan, S.; Sixou, P. *Polymer* **1982**, *23*, 1755.
(23) Daňhelka, J.; Netopilík., M.; Bohdanecký, M. *J. Polym. Sci., Part B: Polym. Phys.* **1987**, *25*, 1801.
(24) Tsuboi, A.; Yamasaki, M.; Norisuye, T.; Teramoto, A. *Polym. J.* **1995**, *27*, 1219.
(25) Jinbo, Y.; Sato, T.; Teramoto, A. *Macromolecules* **1994**, *27*, 6080.
(26) Sakurai, K.; Ochi, K.; Norisuye, T.; Fujita, H. *Polym. J.* **1984**, *16*, 559.
(27) Murakami, H.; Norisuye, T.; Fujita, H. *Macromolecules* **1980**, *13*, 345.
(28) Fujita, H. *Polymer Solutions*; Elsevier: Amsterdam, 1990; Vol. 9.
(29) Konishi, T.; Yoshizaki, T.; Yamakawa, H. *Macromolecules* **1991**, *24*, 5614.
(30) Norisuye, T.; Fujita, H. *Chemtracts Macromol. Chem.* **1991**, *2*, 293.
(31) Benoit, H.; Doty, P. M. *J. Phys. Chem.* **1953**, *57*, 958.
(32) Yamakawa, H.; Shimada, J. *J. Chem. Phys.* **1985**, *83*, 2607.
(33) Shimada, J.; Yamakawa, H. *J. Chem. Phys.* **1986**, *85*, 591.
(34) Yamakawa, H.; Fujii, M. *Macromolecules* **1973**, *6*, 407.
(35) Yamakawa, H.; Fujii, M. *Macromolecules* **1974**, *7*, 128.
(36) Yamakawa, H.; Yoshizaki, T. *Macromolecules* **1979**, *12*, 32.
(37) Yamakawa, H.; Yoshizaki, T. *Macromolecules* **1980**, *13*, 633.
(38) Zugenmaier, P.; Vogt, U. *Makromol. Chem.* **1983**, *184*, 1749.
(39) Norisuye, T.; Tsuboi, A.; Sato, T.; Teramoto, A. *Macromol. Symp.* **1997**, *120*, 65.
(40) Shanbhag, V. P.; Öhman, J. *Ark. Kem.* **1968**, *29*, 163.
(41) Our $[\eta]$ results for CTC samples in dioxane, recently measured, showed almost the same molecular weight dependence as that in THF, and do not agree with a stronger molecular weight dependence of $[\eta]$ for CTC in dioxane reported by Burchard and Husemann.[11] Thus, Daňhelka et al.'s q of CTC in dioxane (=13.5 nm)[23] estimated from the data of Burchard and Husemann may be overestimated.
(42) Schulz, G. V.; Penzel, E. *Makromol. Chem.* **1968**, *112*, 260.
(43) Laivins, G. V.; Gray, G. D. *Macromolecules* **1985**, *18*, 1746.
(44) Conio, G.; Bianchi, E.; Ciferri, A.; Tealdi, A.; Aden, M. A. *Macromolecules* **1983**, *16*, 1264.
(45) Kamide, K.; Miyazaki, Y.; Abe, T. *Polym. J.* **1979**, *7*, 523.
(46) Itou, T. Private communication.
(47) Arai, T.; Abe, F.; Yoshizaki, T.; Einaga, Y.; Yamakawa, H. *Macromolecules* **1995**, *28*, 3609.
(48) Norisuye, T.; Tsuboi, A.; Teramoto, A. *Polym. J.* **1996**, *28*, 357.

MA991443U